Applied Thermal Engineering 188 (2021) 116606

Contents lists available at ScienceDirect

Applied Thermal Engineering

journal homepage: www.elsevier.com/locate/apthermeng

Comparative analysis of evaporation of isobutane (R600a) and propylene (R1270) in compact smooth and microfinned tubes

Ehsan Allymehr [a,*], Ángel Álvarez Pardiñas [b], Trygve Magne Eikevik [a], Armin Hafner [a]

[a] Department of Energy and Process Engineering, NTNU Norwegian University of Science and Technology, Kolbjørn Hejes vei 1D, 7491 Trondheim, Norway
[b] SINTEF Energy Research, Kolbjørn Hejes vei 1, 7491 Trondheim, Norway

ARTICLE INFO

Keywords:
Hydrocarbon
Refrigeration
Heat transfer
Pressure drop
Microfinned

ABSTRACT

Data base for evaporation of flowing isobutane and propylene in compact internally enhanced surfaces is extended by experimental tests in two microfinned tubes and a smooth tube. The outer diameter for all of the test tubes was 5 mm. Heat transfer coefficient and pressure drop were compared for both fluids in all tubes in comparable working conditions. Test conditions were saturation temperatures of 5, 10 and 20 °C, heat fluxes ranging between 15 and 34 k W m^{-2} and mass fluxes between 200 and 515 kg m^{-2} s^{-1}. Results show that propylene has a higher heat transfer coefficient and lower pressure drop compared to isobutane. Furthermore, propylene is nucleate boiling dominant while convective heat transfer is dominant for isobutane. The tested microfinned tubes tend to have a maximum heat transfer coefficient. While for smooth tube correlations were found to reliably predict both heat transfer coefficient and pressure drop, the accuracy of correlations for microfinned tubes is shown to be greatly dependent on the testing conditions and tubes.

1. Introduction

Currently the majority of the working fluids used in refrigeration industries have a particularly high global warming potential (GWP). Meanwhile, a progress towards a more environmentally friendly refrigeration industry requires transitioning to working fluids that not only have a low GWP and zero Ozone Depletion Potential (ODP) but are also more energy efficient. Thus, reducing both the direct and indirect impact of refrigeration industry on environment. Historically hydrocarbons have long been used as working fluids in various applications. Propane (R290), isobutane (R600a) and propylene (R1270) are the most used hydrocarbons in small capacity refrigeration units as they offer a favorable saturation curve for different use cases while they have low GWP and zero ODP. However, the use of hydrocarbons in refrigeration systems have been long limited by the concerns about their flammability. One of the most effective ways to decrease potential risk of flammability with hydrocarbons has been to reduce the charge in the system. It has been shown that in the refrigeration systems the majority of charge accumulates in heat exchangers [31] where the fluid is in liquid phase and therefore with a higher density. Therefore, minimizing the volume of a heat exchanger with methods such as the use of microfinned tubes with a high number of fins is essential to increase the capacity of refrigeration systems using hydrocarbon as the working fluid.

Thonon [39] reviewed the literature on hydrocarbon heat transfer in compact heat exchangers noting that there is a need for more experimental data on in-tube flow boiling of hydrocarbons, especially in the case of microfinned tubes. In a more recent review of evaporation and convective condensation of hydrocarbons by Moreira et al. [25], flow characteristics in convectional and micro sized channels from multiple sources are gathered. The authors concluded that essential parameters for system design such as HTC and pressure drop have been studied by a small number of independent laboratories and data for them is scarce, thus a broader experimental database for assessment of hydrocarbon two phase behaviour becomes essential. Prior research on evaporation of hydrocarbons has mainly focused on tubes of around 10 mm [35,17,28]. Lillo et al. [20] studied the vaporization of R290 in a tube with an internal diameter (d_i) of 6 mm at high saturation temperatures. They noted that the main heat transfer mechanism seems to be nucleate boiling, while correlations of Bertsch et al. [2] and Friedel [10] predicted their results for Heat Transfer Coefficient (HTC) and pressure drop most accurately. Longo et al. [22] studied the characteristics of evaporation of R290 and R1270 while comparing them to R404A in a smooth tube with d_i of 4.0 mm, showing that while R404A has a higher HTC, R1270 and R290 enjoy a lower frictional pressure drop. Longo

* Corresponding author.
E-mail address: ehsan.allymehr@ntnu.no (E. Allymehr).

https://doi.org/10.1016/j.applthermaleng.2021.116606
Received 23 September 2020; Received in revised form 12 January 2021; Accepted 16 January 2021
Available online 30 January 2021

Nomenclature

Greek

β	Spiral angle
δ_{30}	Percentage of predicted values with less than 30% error
γ	Fin angle

Roman

d_i	Fin tip diameter for MF tubes, internal diameter for smooth tube [mm]
d_o	Outer diameter [mm]
E	Enhancement Factor [–]
G	Mass flux [kg m^{-2} s^{-1}]
HTC	Heat Transfer Coefficient [k Wm^{-2} k^{-1}]
I	Efficiency index [–]
i_{lg}	Enthalpy of vaporization [k Wm^{-2} K^{-1}]
l_f	Fin height [mm]
m	Mass flow [kg s^{-1}]
$MARD$	Mean Absolute Relative Deviation [–]
MRD	Mean Relative Deviation [–]
n	Number of fins [–]
P	Penalization Factor [–]
P	Pressure [Pa]
P_r	Reduced pressure [–]
Q	Heat input [W]
q	Heat flux [kJ kg^{-1}]
R_x	Heat exchange area ratio to a smooth tube [–]
S	Heat exchange area [m^2]
T	Temperature [°C]
t_w	Wall thickness [mm]
x	Vapor quality [–]

Subscripts

amb	Ambient condition
element	Heating Element
in	Inlet conditions
l	Liquid phase
lg	Liquid to gas phase change
loss	Heat loss to environment
pre	Preheater section
sat	Saturated condition
test	Test section
w	Wall

et al. [23] compared their previous results with evaporation of R600a in the same tube showing that the HTC of R600a is significantly lower than R1270 and R290. Yang et al. [43] performed similar tests for R600a in conjunction with flow visualization in a smooth tube with d_i of 6.0 mm. More recently, de Oliveira et al. [29] studied evaporation of R1270 in a tube with d_i of 1.0 mm noting a dominance of churn and annular-wavy flow, while correlation of Bertsch et al. [2] best predicted the experimental data.

Multiple studies have researched the effect of internally enhanced tubes on evaporation characteristics of different working fluids. Cho & Kim [5] compared the evaporation characteristics of CO_2 in smooth and microfinned tubes with outer diameters (d_o) of 9.52 and 5 mm showing that the HTC in microfinned tubes increased by up to 210%, whilst the pressure drop increase was up to 1.9 times. Celen et al. [4] investigated evaporation of R134a in smooth and microfinned tubes, showing that the pressure drop is increased by up to 3 times while the HTC is increased by 1.9 times. Colombo et al. [8] observed the flow patterns, characteristics of evaporation and condensation of R134a in one smooth and two microfinned tubes showing that in evaporation both microfinned tubes increase the HTC compared to the smooth tube and found no differences among them. Jiang et al. [14] compared evaporation characteristics of R22, R134a, R407C and R410A in a 9.52 mm outer diameter smooth and microfinned tube showing the highest relative increase in HTC to be 1.86 for R22 while highest increase in pressure drop was 1.45 for R407C.

There are few studies dealing with the effect of enhanced surfaces in evaporation of hydrocarbons. Nan & Infante Ferreira [27] studied evaporation and condensation of propane in a smooth, microfinned, and crosshatched tube with d_o of 9.52 mm. Their results showed the increase in HTC seems to be more noticeable at higher mass fluxes and correlations for internally enhanced tubes considerably over predicted their experimental data. Furthermore, Wen et al. [41] studied the boiling of R600a in a tubes with porous inserts showing that while HTC increases compared to a smooth tube, the relative increase of pressure drop is much higher. More recently, Allymehr et al. [1] studied the evaporation of R290 in smooth and two microfinned tubes demonstrating the prevalence of the nucleate boiling heat transfer mechanism. Moreover, the results showed that with the increase of mass flux in microfinned tube, HTC increase is limited while the pressure drop continues to rise, therefore disincentivizing the use of microfinned tubes in high mass fluxes. Correlations for smooth tube predicted HTC and pressure drop reliably, while the correlations for microfinned tubes showed a significant dependency on the type of tube.

Consequently, while there is a number of studies that published experimental data on characteristics of evaporation of refrigerants, there is limited data available for hydrocarbons. Additionally, almost none of the previous experimental works have studied the influence of internally enhanced surfaces. As microfinned tubes are becoming increasingly common due to the potential in volume and charge reduction in hydrocarbon heat exchangers, reliable experimental data are required to properly design and size heat exchangers in applications such as air to air heat pumps or domestic refrigerators. This study contributes to completing the database on characteristics of flow boiling of R600a and R1270 in both smooth and microfinned tubes by experimentally measuring HTC and pressure drop values. The effectiveness of internally enhanced surfaces in different working conditions was studied by comparing flow characteristics of two microfinned tubes with dissimilar internal geometries to a smooth tube at similar working conditions. The two microfinned tubes are supposed to represent a more conventional internally enhanced geometry and a more aggressive increase in internal surface area. All three tested tubes have an outer diameter of 5 mm, they were tested at mass fluxes ranging from 200 to 515 kg m^{-2} s^{-1} and the heat flux ranged from 15 to 34 kW m^{-2}. The experimental results were further compared with relevant correlations to analyze the accuracy of available prediction methods.

2. Experimental setup

The experimental test rig has been previously used for determination of evaporation characteristics and thus documented in Allymehr et al. [1]. A short description of the test rig is given here for the sake of clarity and ease. Fig. 1 shows the schematic of the test rig, where the test fluid is circulated through the system by a gear pump. Mass flow is measured downstream of the pump. By measurement of the pressure and temperature before the preheater and temperature after preheater, the energy required to vaporize the fluid to the desired inlet quality is calculated. This energy is provided to the fluid in the preheater by means of electrical heating controlled by pulse wave modulation. In order to minimize the heat loss, the test section was insulated using perlite and then contained by hard insulation. Before the test section there is an

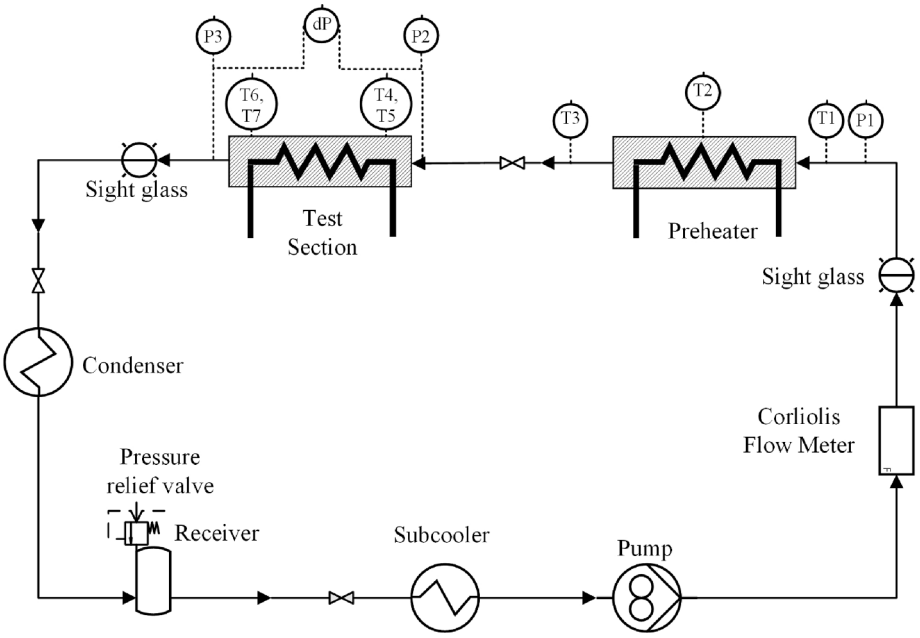

Fig. 1. Test rig schematic.

adiabatic calming section of 75 mm. An electrical heating cable is used as the heating source in the test section. For uniform distribution of heat to the test tube a larger diameter tube is used and the space between the outer tube and the test tube is filled with molten tin. Heat input for both the preheating section and test section is controlled using Pulse Wave Modulation (PWM). The pressure drop is directly measured by a differential pressure transducer via pressures taps 547 mm away from each other at the inlet and outlet of the test section. The wall temperature is obtained from the two pairs of thermocouples brazed to the tube wall located 100 mm from the inlet and outlet of the heated test section. These thermocouples are attached to the outer wall of the test tube by silver brazing. Contact between the thermocouples and the tube is ensured by use silver brazing as it has a higher melting temperature than tin. At each location, one thermocouple is in contact with the top and the other with the bottom part of the test tube. The length of the heated section of all the tested tube is 500 mm. Two pressure sensors are connected to the test section using the same pressure taps for the differential pressure transducer. Average value of these two pressure sensors provides the saturation pressure at test section, and the fluid saturation temperature is determined from this saturation pressure..A photograph of one of the test sections is shown in Fig. 2.

The sight glass located at the exit of the test section does not have the same diameter as tube and therefore is only used for visual inspection of flow. The setup is designed with valves upstream and downstream of the test section, enabling its rapid change without the need to vacuum the whole test rig. At the start-up and with changing of fluids, the test rig is purged with nitrogen and vacuumed before introducing a new fluid. The condenser and the subcooler are each plate heat exchangers. Two separate thermal baths utilizing a secondary fluid are connected to the subcooler and the condenser to ensure a liquid flow to the pump. Moreover, the condenser is located at the lowest point and has the lowest temperature in the system, thus the saturation pressure of the system can be controlled by the temperature of thermal bath connected to the condenser.

2.1. Tested tubes

One smooth tube and two internally enhanced tubes were studied. All three tubes have an d_o of 5 mm. Geometrical parameters are reported in Table 1, and the physical representations of the parameters are presented in Fig. 3. The fin dimensions for the two microfinned tubes, MF1 and MF2, are roughly the same. The MF2 tube has a higher number of fins and spiral angle, which results in a higher available area for heat transfer compared to the other tested tubes. A cross sectional view of the two tested microfinned tubes is shown in Fig. 4.

2.2. Working conditions

Table 2 summarizes the working conditions for both of the fluids. Furthermore, the most differing fluid properties that seem to affect the evaporation characteristics are reported.

2.3. Uncertainty analysis and validation

Uncertainty analysis was carried out by the method elaborated in ISO [13] with a confidence level exceeding 95% (coverage factor of 2).

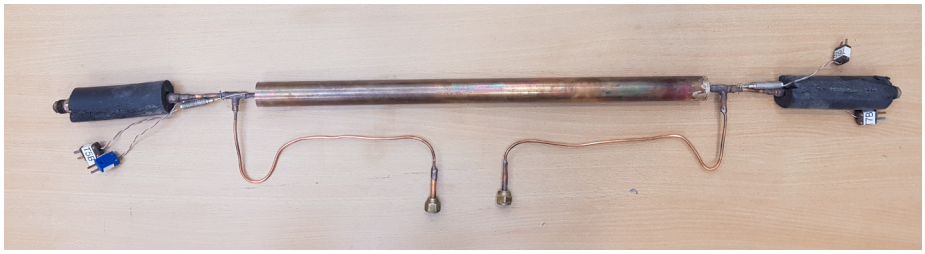

Fig. 2. Photograph of a test section.

Table 1
Geometrical parameters of the test tubes.

	Unit	Smooth tube	MF1	MF2
Outer diameter (d_o)	mm	5	5	5
Fin tip diameter; Internal diameter for smooth tube (d_i)	mm	4.1	4.32	4.26
Wall thickness (t_w)	mm	0.45	0.22	0.22
Actual cross sectional area	mm^2	13.2	15.7	14.8
Fin height (l_f)	mm	–	0.12	0.15
Fin number (n)	(–)	–	35	56
Fin angle (γ)	°	–	35	15
Spiral angle (β)	°	–	15	37
Heat exchange area ratio (R_x)	(–)	1	1.51	2.63
Heated test section length	mm		500	
Pressure drop measurement length	mm		547	
Test section length	mm		1005	

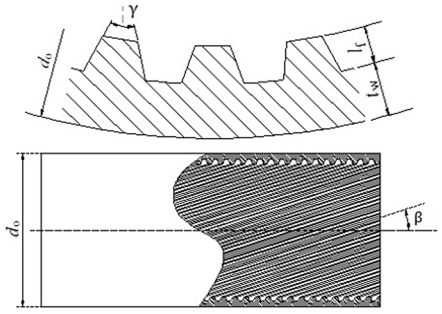

Fig. 3. Physical presentation of the geometrical parameters.

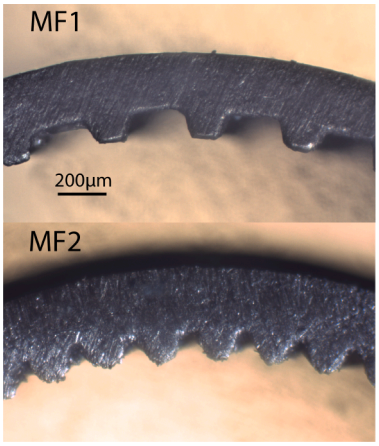

Fig. 4. Cross sectional view of the microfinned tubes.

Utilized instruments are listed in Table 3 with their respective uncertainty. The calibration process and formulation used for uncertainty propagation is documented in Al-lymehr et al. [1]. The average values of the uncertainty of measurement for each studied case are reported in Table 4. The increase of uncertainty for HTC values in microfinned tubes is caused by the smaller temperature differences between the saturation temperature and wall temperature. Furthermore, the higher values of average vapor quality uncertainty for R1270 is caused by the higher random error in the measurement of the mass flow in the highest mass flow. Finally, it can be said that the uncertainty of measurement of pressure drop for R600a is lower, this is because, as it will be seen later, R600a generally has a higher pressure drop and since the differential pressure sensor has a systematic uncertainty of the set span, this will be

Table 2
Operating conditions for experimental setup.

	Unit	Range/Value	
		R1270	R600a
Operating conditions			
Saturation Temperature [T_{sat}]	°C	5, 10	5, 10, 20
Heat flux [q]	kW m^{-2}	15, 24, 33	15, 24, 34
Mass flux [G]	kg m^{-2} s^{-1}	200–515	250–500
Vapor quality [x]	–	0.13–1	0.11–1
Quality change [Δx]	–	0.06–0.14	0.07–0.15
Fluid properties			
Reduced pressure [P_{red}]	–	0.148–0.171	0.051–0.083
Liquid Viscosity at 10 °C	μPa s	110.4	177.5
Surface Tension at 10 °C	m N m^{-1}	8.5	11.8
Vapor Density at 10 °C	kg m^{-3}	16.3	5.9

Table 3
List of instruments and their respective uncertainties.

	Type	Range	Uncertainty
Flow meter	Coriolis	0–5 kg min^{-1}	±0.1% [a]
Absolute pressure sensor	Strain gauge	0–10 bar	±0.16% [b]
Differential pressure sensor	Strain gauge	0–0.5 bar	±0.15% [b]
Thermoucouples	Type T	–	± 0.05 K
Preheater	Electrical	3450 W	±0.44% [a]
Test section heater	Electrical	620 W	± 0.55% [a]

[a] Of the reading.
[b] Of the set span.

Table 4
Average relative total uncertainty of measurement with a confidence level exceeding 95% for each tested tubes and fluid.

	R600a			R1270		
	Smooth	MF1	MF2	Smooth	MF1	MF2
HTC uncertainty [%]	3.5	6.6	9.0	4.3	8.9	8.7
Pressure drop uncertainty [%]	1.5	0.9	1.0	4.8	4.4	4.1
Average Vapor quality uncertainty [%]	1.1	1.2	1.2	4.5	4.6	5.3

percentage-wise smaller for R600a.

The test rig was validated using single phase gas flow of propane flowing through a smooth tube. Pressure drop and HTC were calculated based on Darcy Weisbach formula and the correlation by Gnielinski V. [11], showing an average absolute deviation of 3.7% and 2.6% for pressure drop and heat transfer coefficient, respectively. Vacuum heat leakage tests were performed to account for the heat loss to the environment. Heat loss was taken into account in the data reduction process by a linear relationship based on the difference of ambient and heating element temperature formulated by 1.

$$Q_{loss} = 0.2075 \cdot (T_{element} - T_{amb}) - 0.2925 \quad [W] \tag{1}$$

This heat loss was on average 2.1% of heat input and the maximum value never exceeded 4.3% in highest heat fluxes.

2.4. Data reduction

The four wall temperatures in the last 15 samples should have an standard deviation of less than 0.1 °C for the system to be considered in steady state. If this condition is not met, the system would be considered to be unstable and the data would not be included in the data reduction process. The data from the sensors was recorded for over 120 s to obtain 50 samples, which were then averaged. The average vapor quality value

is calculated by Eq. (2):

$$x = x_{in} + \frac{\Delta x}{2} = \frac{Q_{pre} - \dot{m}\cdot\left(i_{sat,l} - i_1\right)}{\dot{m}\cdot i_{lg(Ppre)}} + \frac{Q_{test} - Q_{loss}}{2\cdot\dot{m}\cdot i_{lg(Psat)}} \quad (2)$$

i_1 is the enthalpy of subcooled fluid before entering the preheater while P_{pre} is the pressure at the preheater section and P_{sat} is the arithmetic average of the inlet and outlet pressure in the test section.

Heat transfer coefficient is calculated using Eq. (3):

$$HTC = \frac{Q_{test} - Q_{loss}}{S\left(\overline{T}_w - \overline{T}_{sat}\right)} \quad (3)$$

Where T_{sat} is derived from the saturation pressure, P_{sat}. $\overline{T}_w$ and S are defined as:

$$\overline{T}_w = \frac{1}{4}\sum_{i=1}^{4} T_{w,i} \quad (4)$$

$$S = \pi d_i L \quad (5)$$

The parameters depending on d_i for the microfinned tubes such as mass flux and heat flux, are calculated based on a smooth tube with internal diameter equal to the fin tip diameter. Thermodynamic properties are evaluated using REFPROP V10 [18].

The total pressure drop ΔP_t is calculated by addition of the momentum pressure ΔP_a drop with frictional pressure drop ΔP_f. The void fraction in the momentum pressure drop calculation was determined using Rouhani & Axelsson [33] correlation. Although this correlation was originally developed for vertical tubes, it takes into account several parameters that are important in mini and micro channels. Therefore it has been used in multiple sources for calculation of the void fraction in horizontal tubes [20,29].

3. Results and discussion

3.1. HTC and Pressure drop

Fig. 5 presents the effect of saturation temperature on HTC. The results for the smooth tube show no discernible change for R1270 and R600a. The results for the microfinned tube show a similar pattern, albeit the higher uncertainty levels at higher vapor quality make the comparison less clear.

Fig. 6 depicts the effect of mass flux on HTC in the smooth tube for both of the fluids. The results indicate that R1270 has higher HTC in all the test conditions, although the increase is more pronounced in lower vapor quality. This can be indicative of a more influential convective heat transfer mechanism in R600a, while heat transfer in R1270 is mainly carried out by nucleation boiling process, thus having a relatively milder increase in HTC with increasing vapor quality. This claim can be further supported by thermophysical properties of fluids. Table 2 shows that the surface tension of the R600a is considerably higher than R1270, this is known to suppress the nucleate boiling by increasing the smallest radius for onset of nucleate boiling [36].

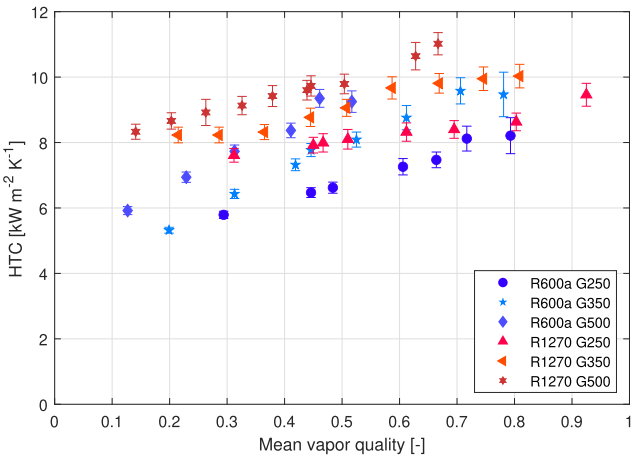

Fig. 6. Effect of mass flux on HTC in smooth tube with q = 24 kW m^{-2}, T_{sat} = 5 °C for R1270 and R600a, mass flux (G) in the legend reported in kg m^{-2} s^{-1}.

Fig. 7 compares HTC of R1270 and R600a in microfinned tubes in different mass fluxes. Tube MF1 exhibits a clear distinction between fluids, as R1270 has a higher HTC compared to R600a and this increases with the vapor quality. This can be explained by arguing that the microfinned tubes enhance the convective heat transfer regime for R1270, while R600a is already benefiting from a convective energy transport, thus not enhancing the HTC in the same way. As for the MF2, it seems that the HTC is relatively higher for both of the fluids compared to MF1 in similar conditions, this increase is more noticeable at higher vapor qualities and for R600a. The effect of mass flux on HTC seems to be minute for both of the fluids. This upper limit in increase of HTC with mass flux for microfinned tubes was also observed in previous tests for R290 [1]. It can be speculated that the independence of HTC values from

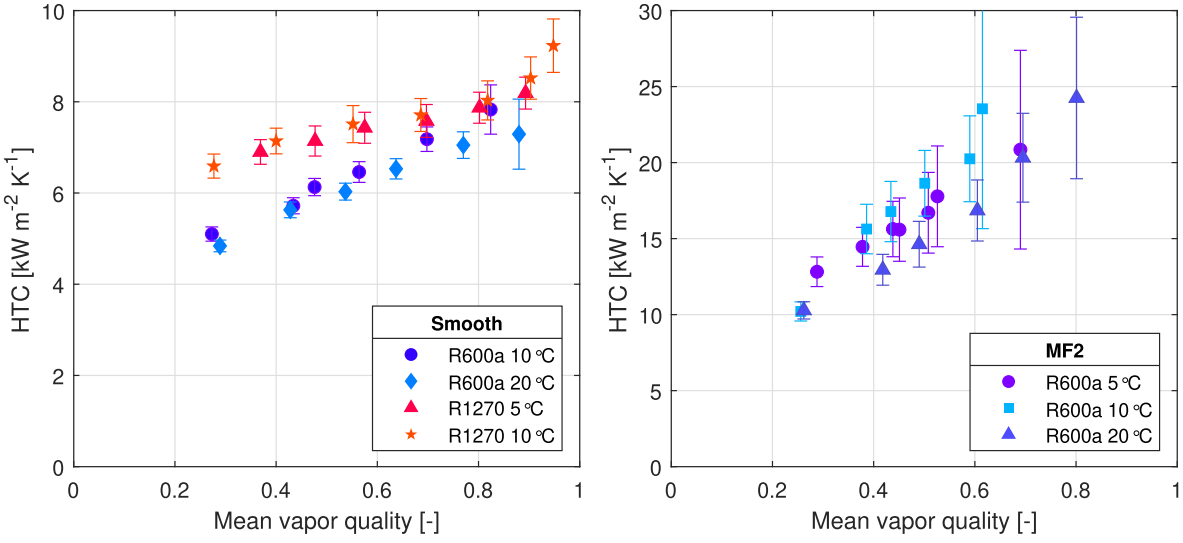

Fig. 5. Effect of saturation temperature on HTC for R1270 and R600a, G = 250 kg m^{-2} s^{-1},q = 15 kW m^{-2}.

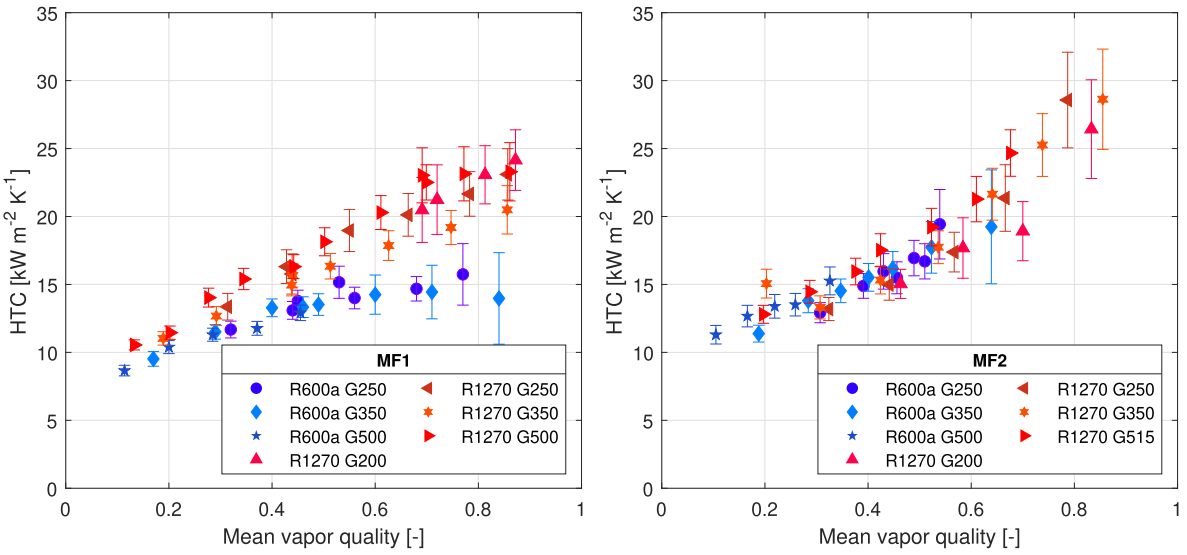

Fig. 7. Effect of mass flux on HTC on MF1 and MF2 with q = 24 kW m^{-2}, T_{sat} = 5 °C for R1270 and R600a, mass flux (G) reported in the legend in kg m^{-2} s^{-1}.

mass flux is caused by the high spiral angle. With increasing mass flux the velocity of the gas core increases, but the increased longitudinal vapor flow cannot increase the swirl motion in liquid film between the fins, as the speed vectors of the phases are notably different from each other. The increased mass flux for isobutane caused the two phase instabilities to happen in lower vapor qualities. Maximum reported values of vapor quality for R600a are lower for higher mass fluxes, this is because unstable points are not reported.

The effect of heat flux on HTC of both fluids in smooth tube is presented in Fig. 8. As expected, since the nucleate boiling effect is dominant for R1270, the HTC increases dramatically with higher heat fluxes in lower vapor quality region, while R600a does not seem to benefit from an increase in the heat flux in a noticeable way.

Fig. 9 shows the effect of heat flux on the HTC of microfinned tubes. HTC values for evaporation of R600a in the MF1 tube seem to be independent of the heat flux. As for R1270 in MF1 tube, there is a considerable increase in HTC going from the lowest heat flux to the average heat flux in all vapor quality ranges. For the highest heat flux, the HTC increased in low vapor quality regions, while in higher vapor quality regions, the HTC is lower than the average heat flux. This trend is remarkable and can be seen in the MF2 tube for R1270 as well, albeit to a lesser extent. While the underlying reason for this remains unclear and would require flow visualization tests, it is probable that the high heat fluxes at relatively low vapor qualities are able to create local dryout in the tube, while other parts of the tube are still in contact with liquid phase. This trend has also been reported for R290 [1]. Finally, the results for the MF2 tube seem to be somewhat independent of the applied heat flux or the fluid used. It could be speculated that the increase of the HTC decreases the wall temperature, suppressing nucleate boiling and eliminating the effect of heat flux in heat transfer. Seemingly the same mechanism controls the evaporation of R600a in MF1 tube. This results indicate again the limitations for increase of heat transfer by use of microfinned tubes.

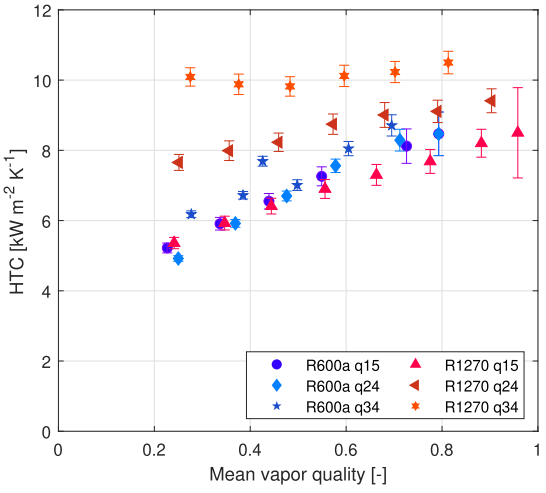

Fig. 8. Effect of heat flux on HTC on smooth tube with G = 300 kg m^{-2} s^{-1}, T_{sat} = 10 °C, reported heat flux (q) in kW m^{-2}.

The pressure drop is strongly dependent on the mass flux. This can be seen in Fig. 10, which presents the data for the pressure gradient in the smooth tube. R1270 has a lower pressure gradient for all the tested conditions compared to R600a. This is unsurprising as the liquid viscosity of R600a is considerably greater than R1270, meanwhile the vapor density for R600a is lower compared to R1270, creating a higher gas velocity that contributes to a higher shear stress. Furthermore, the results show that R600a is slightly more sensitive to the increase of the mass flux. Finally, R600a is influenced more by the higher vapor quality in higher mass fluxes. (see Fig. 11).

In order to compare the effect of MF tubes, three parameters are defined, Enhancement factor E, Penalization factor P, and efficiency index, I, which are formulated as:

$$E = \frac{h_{MF}}{h_{Smooth}} \tag{6}$$

$$P = \frac{\Delta P_{MF}}{\Delta P_{Smooth}} \tag{7}$$

$$I = \frac{E}{P} \tag{8}$$

These factors are visualized in Fig. 12 for both of the fluids. The data could not be obtained for all the mass fluxes because of difficulties in accurate control of mean vapor quality or limitations of instruments specially for R1270 flowing in MF2 tube, nevertheless the figures present a clear pattern for all the three parameters apart from R1270 in MF2. Enhancement factor, E, decreases with mass flux for all the tested cases. As mentioned earlier this happens mainly because of the increase in HTC of smooth tube in higher mass fluxes while MF tubes present a more or less constant HTC with mass flux. It is also interesting to compare the value of E with the increase in heat exchange area, R_x, it

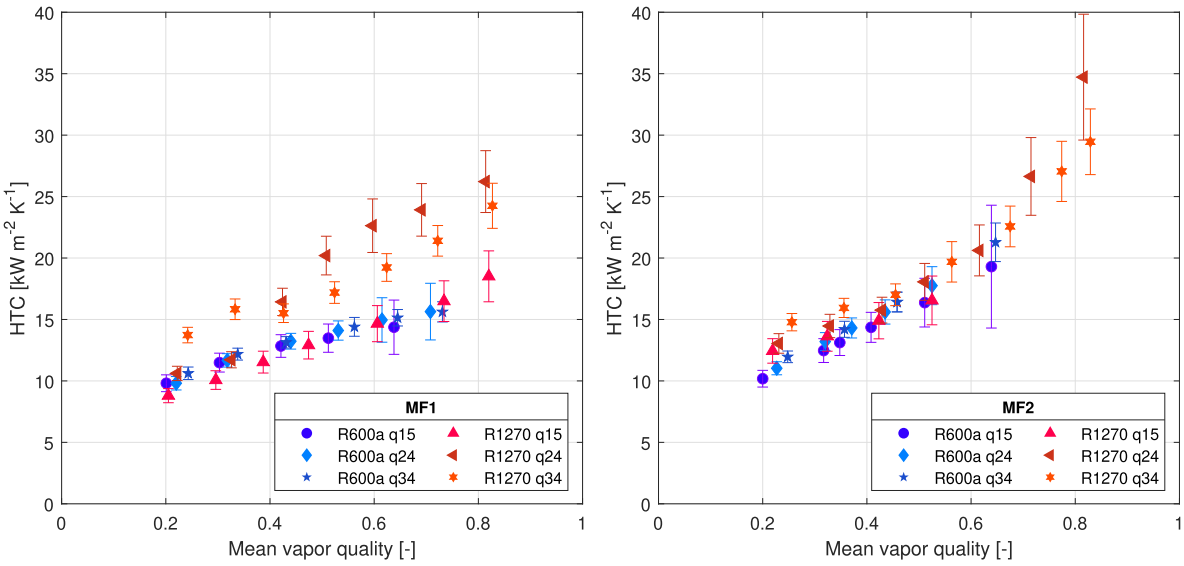

Fig. 9. Effect of heat flux on HTC in microfinned tubes with G = 300 kg m^{-2} s^{-1}, T_{sat} = 10 °C, reported heat flux (q) in kW m^{-2}.

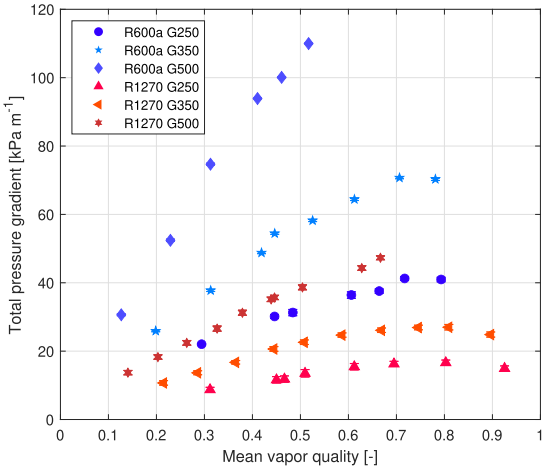

Fig. 10. Effect of mass flux on total pressure gradient of smooth tube at q = 24 kW m^{-2} for R1270 and R600a, mass flux (G) reported in the legend in kg m^{-2} s^{-1}.

seems that for MF1 tube E is higher than R_x in lower mass fluxes, while in higher mass fluxes E moves asymptotically towards R_x. In MF2 tube E is lower than R_x and it further reduces in higher mass fluxes. This can be explained by arguing that in low mass fluxes the turbulence caused by the fins would affect the thermal boundary layer at the wall and increase the HTC, while in the higher mass fluxes the turbulence at smooth tube would compensate for this. Nevertheless the increase in the heat transfer area enables more heat to be transferred from the fluid in MF tubes in this condition. The results for MF2 tube also indicate that while a higher increase in the heat transfer area is beneficial for HTC, this increase is not linear and diminishing. Value of E for R1270 in MF2 seems to be an outlying point, as the increase of HTC is lower than expected. While the number of available data points is too small to make a verdict, it could be argued that although the increased turbulence would increase the HTC, the higher spiral angle, β, could suppress the nucleate boiling which is the dominant heat transfer mechanism for R1270. As for penalization factor, P, it is higher for MF2 tube. This was expected because of the higher fin number and spiral angle of the MF2 tube. Furthermore, P does not seem to be a function of mass flux. Finally regarding the efficiency index, I, there is a clear decrease with mass flux. If efficiency index were to be considered as how advantageous is the use of an internally

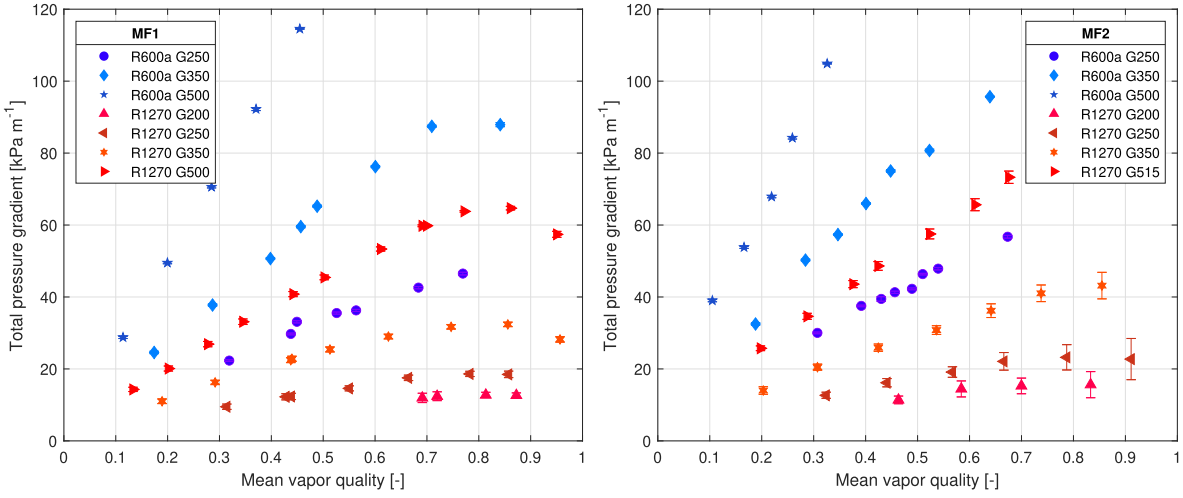

Fig. 11. Effect of mass flux on total pressure gradient of R1270 and R600a at q = 24 kW m^{-2}, T_{sat} = 5 °C for MF1 and MF2, mass flux (G) in legend reported in kg m^{-2} s^{-1}.

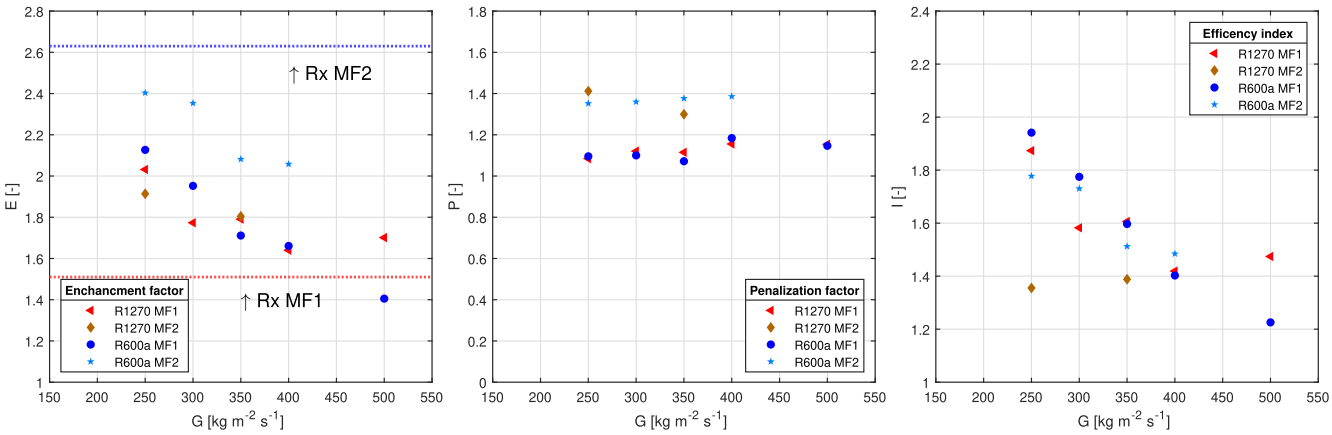

Fig. 12. Enhancement factor E, Penalization factor P and efficiency index, I as a function of mass flux, q = 23 kW m^{-2},T_{sat} = 5 °C, x = 0.45, heat exchange area increase shown with R_x.

enhanced tube, it could be concluded that the microfinned tubes are most beneficial in low mass fluxes. Interestingly with a higher E and P value, the efficiency index of MF2 tube is close to MF1 tube. Thus from this point of view, there is no difference between these internally enhanced tubes. Nevertheless, if the goal of heat exchanger design were to minimize the charge, it would still be favorable to use a tube with a higher number of fins and spiral angle, such as MF2 tube.

3.2. Correlations

The experimental data for HTC and pressure drop for all tested conditions are compared with applicable predictive correlations by values of Mean Relative Deviation (MRD) and Mean Absolute Relative Deviation (MARD), defined as:

$$MRD = \frac{100}{n}\sum_{i=1}^{n}\frac{Predicted_i - Experimental_i}{Experimental_i} \quad (9)$$

$$MARD = \frac{100}{n}\sum_{i=1}^{n}\left|\frac{Predicted_i - Experimental_i}{Experimental_i}\right| \quad (10)$$

Furthermore, δ_{30} is defined as the percentage of the predicted values having less than 30% deviation from the experimental data. Table 5 shows the values of MRD, MARD and δ_{30} of the selected correlations for the smooth tube.

Special care was taken to choose correlations that are most applicable to the experimental condition of this study, for example, all the studied correlations for the evaluation of pressure drop in smooth tube use dimensionless quantities such as Laplace or Weber number to account for the effect of surface tension, except Müller-Steinhagen & Heck [26]. The selection of HTC correlations was focused either on correlations developed for hydrocarbons such as Mohd-Yunos et al. [24] or those considering smaller-diameter tubes such as Bertsch et al. [2]. Furthermore, well known correlations such as Kandlikar [15] and Liu & Winterton [21] were also analyzed. Table 5 summarizes the results of comparison for both of the fluids in smooth tube.

Apart from Sun & Mishima [37], the selected correlations for pressure drop in smooth tube show a high degree of reliability in predicting experimental results, data was most accurately predicted by Xu & Fang [42] confirming the prior results for pressure drop in R290 [1]. In Xu & Fang [42] authors studied correlations and experimental data of 15 different fluids in tubes with hydraulic diameters between 0.81 and 19.1 mm and developed a correlation improving the accuracy especially for micro-channels. Notably this correlation did not have any hydrocarbons in it's database. The parity plot for this correlation is shown in Fig. 13.

As for the HTC, correlation of Mohd-Yunos et al. [24] and Lillo et al.

Table 5
Comparison between experimental results and correlations for HTC and pressure drop in smooth tube.

	R600a			R1270		
	MRD %	MARD %	δ_{30}	MRD %	MARD %	δ_{30}
Pressure Drop Correlations						
Müller-Steinhagen & Heck [26]	−13.1	15.6	100	−16.7	19.4	97
Sun & Mishima [37]	−33.0	33.0	28.6	−33.4	33.4	20.9
Cavallini et al. [3]	3.0	12.7	90.0	−10.6	20.6	92.5
Xu & Fang [42]	1.8	6.6	100	−5.3	9.9	100
Friedel [10]	−20.1	20.4	94.3	−17.1	18.6	100
HTC Correlations						
Choi et al. [7]	1.2	15.2	88.1	0.9	24.8	80.6
Liu & Winterton [21]	15.3	15.3	90.0	6.8	8.5	100
Kandlikar [15]	19.8	19.8	90.0	−3.2	9.2	100
Tran et al. [40]	−59.0	59.0	1.4	−48.5	48.5	1.5
Gungor & Winterton [12]	9.8	12.5	94.3	4.3	9.4	97.0
Shah [34]	1.7	6.4	100	−17.5	18.5	88.1
Li & Wu [19]	−52.3	52.3	4.3	−36.1	36.1	28.4
Kim & Mudawar [16]	−29.4	29.4	51.4	−16.8	17.7	89.6
Bertsch et al. [2]	−42.3	42.3	14.3	−40.2	40.2	31.3
Mohd-Yunos et al. [24]	−52.7	52.7	5.7	−46.0	46.0	7.5
Lillo et al. [20]	30.1	30.7	71.4	92.2	92.2	55.2

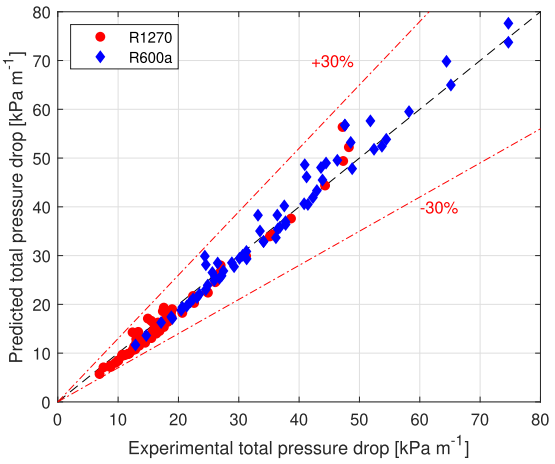

Fig. 13. Comparison between experimental data and correlations of Xu & Fang [42] for prediction of pressure drop of R600a and R1270. in smooth tube.

[20] which were explicitly developed for hydrocarbons using genetic algorithms and flow pattern observation respectively, were surprisingly the least reliable correlations. Correlation of Lillo et al. [20] is intriguing as it shows a sound agreement with experimental results in lower vapor qualities, while at higher vapor qualities over predicts the experimental data. Therefore it seems that Lillo et al. [20] emphasizes the effect of convective heat transfer, and consequently it can follow R600a experimental data more closely as the heat transfer mechanism for R600a is convection dominated.

Correlations of Liu & Winterton [21], Kandlikar [15], Gungor & Winterton [12] performed best in predicting the HTC, being able to predict more than 90% of data points with less than 30% error for both of the fluids. Almost all of these correlation are relying on the principle of dividing the boiling heat transfer in two parts, nucleate boiling and convective boiling, thus the difference between them arises from how some factors are defined based on the database used for their development. This is again similar to the results obtained for R290 in Allymehr et al. [1].

Microfinned tube correlations were calculated using the formulation provided in their respective papers. If the formulation used for microfinned correlations utilized parameter definitions other than the ones used in this study, experimental data was converted to match the correlation's definition. This point is crucial in choice of internal diameter as it affects other parameters such as mass flux, G and heat transfer area, S.

Table 6 shows the comparison data for MF1 tube for pressure drop and HTC. While Diani et al. [9] predicts R1270 data the best and Rollmann & Spindler [32] does so for R600a data, it can be said that both are capable of accurately predicting the pressure drop for both of the fluids.

As for HTC, the correlation of Padovan et al. [30] is the most accurate in both fluids, albeit the reliability is less for R1270 compared to R600a. This is even more notable for the correlation of Rollmann & Spindler [32] where δ_{30} drops from 95.5% for R600a to 3.5% for R1270. This can be explained by arguing that the Prandtl number of R1270 in tested condition is close to the range of validity declared in Rollmann & Spindler [32] to be higher than 2.28, while R600a fits better in the range of validity.

Results for MF2 tube portrayed in Table 7 show that while Diani et al. [9] reliably predicts the pressure drop, other correlations perform significantly worse compared to MF1 tube data. Furthermore, none of the correlation seem to be able to follow the HTC of MF2 tube. While the correlation of Tang & Li [38], Rollmann & Spindler [32] show the lowest values of MRD and MARD, their predictive ability is far lower for R1270 compared to R600a. The lower availability of data for R1270 as a working fluid might be the a contributing factor for this inconsistency. The parity plot in Fig. 14 visualizes the comparison between the correlations of Rollmann & Spindler [32], Diani et al. [9] and the experimental data for MF1 and MF2.

Table 6
Comparison between experimental data and correlations for prediction of HTC and pressure drop for microfinned tube MF1.

	R600a MF1			R1270 MF1		
	MRD %	MARD %	δ_{30}	MRD %	MARD %	δ_{30}
Pressure Drop Correlations						
Choi et al. [6]	−15.9	15.9	100	28.7	28.8	41.4
Rollmann & Spindler [32]	−3.8	5.7	100	−9.6	13.2	96.6
Diani et al. [9]	13.9	13.9	100	−3.3	5.2	100
HTC Correlations						
Tang Li [38]	−36.9	36.9	31.8	−28.1	29.4	53.4
Rollmann & Spindler [32]	1.7	12.0	95.5	−58.8	58.8	3.5
Diani et al. [9]	−35.4	35.4	11.4	−28.6	28.9	56.9
Padovan et al. [30]	1.0	5.4	100	19.6	23.4	74.1

Table 7
Comparison between experimental data and correlations for prediction of HTC and pressure drop for microfinned tube MF2.

	R600a MF2			R1270 MF2		
	MRD %	MARD %	δ_{30}	MRD %	MARD %	δ_{30}
Pressure Drop Correlations						
Choi et al. [6]	29.5	29.5	47.2	18.9	18.9	85.4
Rollmann & Spindler [32]	−30.3	30.3	41.5	−32.6	32.6	33.3
Diani et al. [9]	−4.0	4.4	100	−14.8	14.8	100
HTC Correlations						
Tang & Li [38]	23.4	23.4	73.6	41.4	41.4	25.0
Rollmann & Spindler [32]	−25.6	25.6	69.8	−65.6	65.6	0
Diani et al. [9]	56.6	56.6	3.8	85.2	85.2	4.2
Padovan et al. [30]	113.2	113.2	0.0	168.1	168.1	0.0

Finally, a cross examination of Tables 6 and 7 shows that the predictive ability for HTC of Padovan et al. [30], Diani et al. [9] is significantly worse for MF2 data. A closer analysis of these correlations shows that the heat exchange area multiplier in these correlations were designed for tubes with a low increase in heat exchange area ratio, such as in MF1 tube, hence over predicting HTC data for MF2.

4. Conclusion

While microfinned tubes have the potential to reduce volume and charge in heat exchangers, lack of data for key design elements makes system design challenging. This paper contributes to the available literature on flow characteristics of hydrocarbons by presenting experimental data on evaporation of isobutane (R600a) and propylene (R1270) in one smooth and two microfinned tubes with an outer diameter of 5 mm. The increased heat exchange area for microfinned tubes are 1.51 and 2.63 for MF1 and MF2, respectively. The characteristics of flow in two microfinned tubes and the smooth tube are compared in similar working conditions. Experimental data was recorded at saturation temperatures 5, 10 and 20 °C, heat fluxes ranging between 15 and 34 kW m^{-2} and mass fluxes from 200 to 515 kg m^{-2} s^{-1}.

The results are critically compared, noting that saturation temperature does not strongly affect the HTC. In similar test conditions, R1270 has a higher HTC and a lower pressure drop than R600a. With increasing heat flux, HTC of R1270 increases in smooth tube and MF1 tube, specially at lower vapor qualities indicating a prevalence of nucleate boiling regime, while R600a is not affected. With increasing mass flux, HTC in smooth tube for both R600a and R1270 increases at higher vapor qualities. As for the MF2 tube, HTC values remain the same with increasing mass flux and heat flux, showing a maximum heat transfer capability. As for the pressure drop, the most decisive parameter for all fluids and tubes is the mass flux. Comparison of data between MF tubes and smooth tube showed a maximum increase of 2.4 and 2.0 for HTC of R600a and R1270, respectively. Increase of pressure drop in MF tubes were 1.15 and 1.4 for MF1 and MF2 tube, respectively. Since by increasing mass flux the relative increase in pressure drop between microfinned and smooth tubes is greater than the relative increase in HTC, the use of microfinned tubes in higher mass fluxes is discouraged.

Finally, the experimental data has been compared with several predictive correlations available in the literature. For smooth tube, correlations of Xu & Fang [42] and Liu & Winterton [21] reliably predict pressure drop and HTC, respectively. For microfinned tubes, accuracy of the prediction methods varied based on the tested tube and the fluid. Correlation of Diani et al. [9] reliably predicted all pressure drop experimental data. Correlation of Rollmann & Spindler [32] best predicted the HTC data for R600a, while there were no reliable correlation found for HTC of R1270.

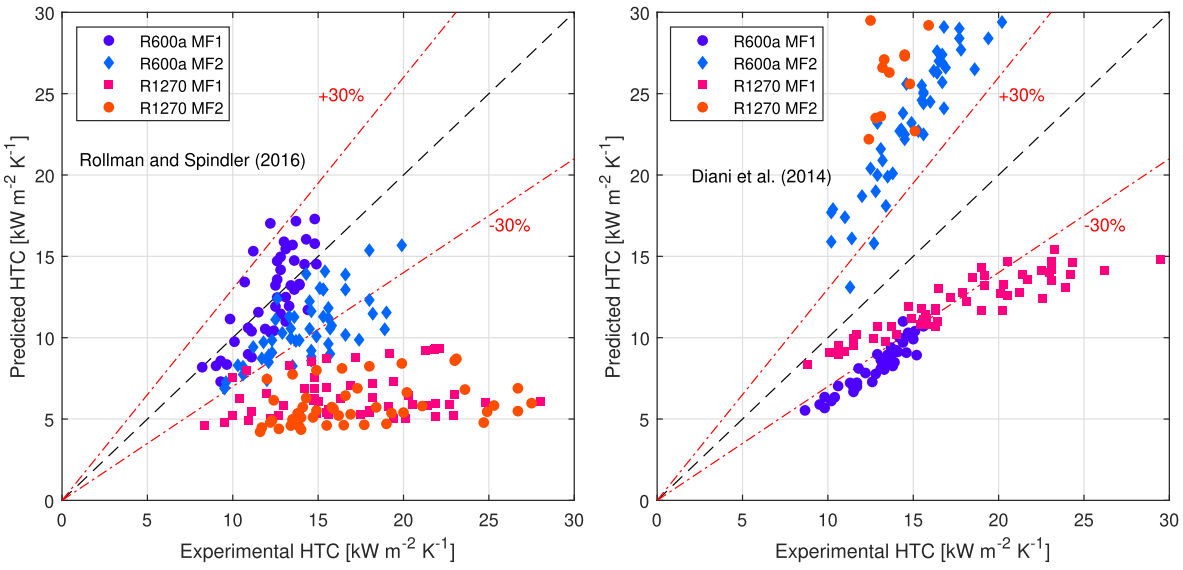

Fig. 14. Prediction of HTC in two microfinned tubes by correlations of Diani et al. [9] and Rollmann & Spindler [32] compared to experimental data.

Declaration of Competing Interest

The authors declare that they have no known competing financial interests or personal relationships that could have appeared to influence the work reported in this paper.

Acknowledgments

This publication has been funded by HighEFF - Centre for an Energy Efficient and Competitive Industry for the Future, an 8-years' Research Centre under the FME-scheme (Centre for Environment-friendly Energy Research, 257632). The authors gratefully acknowledge the financial support from the Research Council of Norway and user partners of HighEFF.

References

[1] E. Allymehr, Á.Á. Pardiñas, T.M. Eikevik, A. Hafner, Characteristics of evaporation of propane (R290) in compact smooth and microfinned tubes, Appl. Therm. Eng. 181 (2020) 115880, https://doi.org/10.1016/j.applthermaleng.2020.115880.
[2] S.S. Bertsch, E.A. Groll, S.V. Garimella, A composite heat transfer correlation for saturated flow boiling in small channels, Int. J. Heat Mass Transf. 52 (2009) 2110–2118, https://doi.org/10.1016/j.ijheatmasstransfer.2008.10.022.
[3] A. Cavallini, G. Censi, D.D. Col, L. Doretti, G. Longo, L. Rossetto, Condensation of Halogenated Refrigerants Inside Smooth Tubes, HVAC&R Res. 8 (2002) 429–451, https://doi.org/10.1080/10789669.2002.10391299, http://www.tandfonline.com/doi/abs/10.1080/10789669.2002.10391299.
[4] A. Celen, A. Çebi, A.S. Dalkiliç, Investigation of boiling heat transfer characteristics of R134a flowing in smooth and microfin tubes, Int. Commun. Heat Mass Transfer 93 (2018) 21–33, https://doi.org/10.1016/j.icheatmasstransfer.2018.03.006.
[5] J.M. Cho, M.S. Kim, Experimental studies on the evaporative heat transfer and pressure drop of CO2 in smooth and micro-fin tubes of the diameters of 5 and 9.52 mm, Int. J. Refrig. 30 (2007) 986–994, https://doi.org/10.1016/j.ijrefrig.2007.01.007.
[6] J.Y. Choi, M.A. Kedzierski, P.A. Domanski, Generalized Pressure Drop Correlation for Evaporation and Condensation in Smooth and Micro-Fin Tubes, IIF-IIR-Commission B1 (2001) http://fire.nist.gov/bfrlpubs/build01/PDF/b01078.pdf.
[7] K.-I. Choi, A. Pamitran, C.-Y. Oh, J.-T. Oh, Boiling heat transfer of R-22, R-134a, and CO2 in horizontal smooth minichannels, Int. J. Refrig. 30 (2007) 1336–1346, https://doi.org/10.1016/j.ijrefrig.2007.04.007, https://www.sciencedirect.com/science/article/pii/S014070070700076X?via%3Dihub https://linkinghub.elsevier.com/retrieve/pii/S014070070700076X. doi:10.1016/j.ijrefrig.2007.04.007.
[8] L. Colombo, A. Lucchini, A. Muzzio, Flow patterns, heat transfer and pressure drop for evaporation and condensation of R134A in microfin tubes, Int. J. Refrig. 35 (2012) 2150–2165, https://doi.org/10.1016/j.ijrefrig.2012.08.019, https://www.sciencedirect.com/science/article/pii/S014070071200206X?via%3Dihub https://linkinghub.elsevier.com/retrieve/pii/S01407007120020.
[9] A. Diani, S. Mancin, L. Rossetto, R1234ze(E) flow boiling inside a 3.4 mm ID microfin tube, Int. J. Refrig. 47 (2014) 105–119, https://doi.org/10.1016/j.ijrefrig.2014.07.018.
[10] L. Friedel, Improved friction pressure drop correlation for horizontal and vertical two-phase pipe flow, in: European Two-Phase Flow Group Meeting, Ispra, 1979, pp. 485–492.
[11] V. Gnielinski, New equations for heat and mass transfer in the turbulent flow in pipes and channels, Forsch. Ingenieurwes. 41 (1975) 8–16, http://adsabs.harvard.edu/abs/1975STIA...7522028G.
[12] K. Gungor, R. Winterton, A general correlation for flow boiling in tubes and annuli, Int. J. Heat Mass Transf. 29 (1986) 351–358, https://doi.org/10.1016/0017-9310(86)90205-X, http://linkinghub.elsevier.com/retrieve/pii/001793108690205X.
[13] ISO, 1993. Guide to Expression of Uncertainty in Measurement.
[14] G.B. Jiang, J.T. Tan, Q.X. Nian, S.C. Tang, W.Q. Tao, Experimental study of boiling heat transfer in smooth/micro-fin tubes of four refrigerants, Int. J. Heat Mass Transf. 98 (2016) 631–642, https://doi.org/10.1016/j.ijheatmasstransfer.2016.03.024.
[15] S.G. Kandlikar, A General Correlation for Saturated Two-Phase Flow Boiling Heat Transfer Inside Horizontal and Vertical Tubes, J. Heat Transf. 112 (1990) 219, https://doi.org/10.1115/1.2910348.
[16] S.-M. Kim, I. Mudawar, Review of databases and predictive methods for heat transfer in condensing and boiling mini/micro-channel flows, Int. J. Heat Mass Transf. 77 (2014) 627–652, https://doi.org/10.1016/j.ijheatmasstransfer.2014.05.036.
[17] H. Lee, J. Yoon, J. Kim, P. Bansal, Evaporating heat transfer and pressure drop of hydrocarbon refrigerants in 9.52 and 12.70mm smooth tube, Int. J. Heat Mass Transf. 48 (2005) 2351–2359, https://doi.org/10.1016/j.ijheatmasstransfer.2005.01.012, http://linkinghub.elsevier.com/retrieve/pii/S0017931005001158.
[18] E.W. Lemmon, I.H. Bell, M.L. Huber, M.O. McLinden, NIST Standard Reference Database 23: Reference Fluid Thermodynamic and Transport Properties-REFPROP, Version 10.0, National Institute of Standards and Technology, 2018. https://www.nist.gov/srd/refprop. doi:https://dx.doi.org/10.18434/T4JS3C.
[19] W. Li, Z. Wu, A general criterion for evaporative heat transfer in micro/mini-channels, Int. J. Heat Mass Transf. 53 (2010) 1967–1976, https://doi.org/10.1016/j.ijheatmasstransfer.2009.12.059.
[20] G. Lillo, R. Mastrullo, A.W. Mauro, L. Viscito, Flow boiling heat transfer, dry-out vapor quality and pressure drop of propane (R290): Experiments and assessment of predictive methods, Int. J. Heat Mass Transf. 126 (2018) 1236–1252, https://doi.org/10.1016/j.ijheatmasstransfer.2018.06.069.
[21] Z. Liu, R.H. Winterton, A general correlation for saturated and subcooled flow boiling in tubes and annuli, based on a nucleate pool boiling equation, Int. J. Heat Mass Transf. 34 (1991) 2759–2766, https://doi.org/10.1016/0017-9310(91)90234-6, http://linkinghub.elsevier.com/retrieve/pii/0017931091902346.
[22] G.A. Longo, S. Mancin, G. Righetti, C. Zilio, Hydrocarbon refrigerants HC290 (Propane) and HC1270 (Propylene) low GWP long-term substitutes for HFC404A: A comparative analysis in vaporisation inside a small-diameter horizontal smooth tube, Appl. Therm. Eng. 124 (2017) 707–715, https://doi.org/10.1016/j.applthermaleng.2017.06.080.
[23] G.A. Longo, S. Mancin, G. Righetti, C. Zilio, Hydrocarbons vaporization inside a 4 mm ID horizontal. In: 13th IIR-Gustav Lorentzen Conference on Natural Refrigerants:. Valencia, 2018. doi:10.18462/iir.gl.2018.1329.
[24] Y. Mohd-Yunos, N. Mohd-Ghazali, M. Mohamad, A.S. Pamitran, J.-T. Oh, 2019. Improvement of two-phase heat transfer correlation superposition type for propane by genetic algorithm. Heat and Mass Transfer, http://link.springer.com/10.1007/s00231-019-02776-x. doi:10.1007/s00231-019-02776-x.
[25] T.A. Moreira, G. Furlan, G.H.d.S.e. Oliveira, G. Ribatski, Flow boiling and convective condensation of hydrocarbons: A state-of-the-art literature review, Appl. Therm. Eng. 182 (2021) 116129, https://doi.org/10.1016/j.

applthermaleng.2020.116129, https://linkinghub.elsevier.com/retrieve/pii/S1359431120336097.
[26] H. Müller-Steinhagen, K. Heck, A simple friction pressure drop correlation for two-phase flow in pipes. Chemical Engineering and Processing: Process Intensification, 20 (1986) 297–308. http://users.ugent.be/ mvbelleg/literatuur SCHX - Stijn Daelman/ORCNext/Supercritical/Literature Study/Literature/Papers SC Heat transfer/Pressure drop-friction/1986 - Muller-Steinhagen - A simp http://linkinghub.elsevier.com/retrieve/pii/0255270186800083. doi:10.1016/0255-2701(86)80008-3.
[27] X.H. Nan, C. Infante Ferreira, In tube evaporation and condensation of natural refrigrant R290 (Propane), Gustav Lorentz conference 290 (2000) 3.
[28] M. Nasr, M. Akhavan-Behabadi, M. Momenifar, P. Hanafizadeh, Heat transfer characteristic of R-600a during flow boiling inside horizontal plain tube, Int. Commun. Heat Mass Transfer 66 (2015) 93–99, https://doi.org/10.1016/j.icheatmasstransfer.2015.05.024, https://linkinghub.elsevier.com/retrieve/pii/S0735193315001037.
[29] J.D. de Oliveira, J.B. Copetti, J.C. Passos, C.W. van der Geld, On flow boiling of R-1270 in a small horizontal tube: Flow patterns and heat transfer, Appl. Therm. Eng. 178 (2020) 115403, https://doi.org/10.1016/j.applthermaleng.2020.115403.
[30] A. Padovan, D. Del Col, L. Rossetto, Experimental study on flow boiling of R134a and R410A in a horizontal microfin tube at high saturation temperatures, Appl. Therm. Eng. 31 (2011) 3814–3826, https://doi.org/10.1016/j.applthermaleng.2011.07.026.
[31] B. Palm, Refrigeration systems with minimum charge of refrigerant, Appl. Therm. Eng. 27 (2007) 1693–1701, https://doi.org/10.1016/j.applthermaleng.2006.07.017, https://linkinghub.elsevier.com/retrieve/pii/S1359431106002481.
[32] P. Rollmann, K. Spindler, New models for heat transfer and pressure drop during flow boiling of R407C and R410A in a horizontal microfin tube, Int. J. Therm. Sci. 103 (2016) 57–66, https://doi.org/10.1016/j.ijthermalsci.2015.11.010.
[33] S.Z. Rouhani, E. Axelsson, Calculation of void volume fraction in the subcooled and quality boiling regions, Int. J. Heat Mass Transf. 13 (1970) 383–393, https://doi.org/10.1016/0017-9310(70)90114-6, http://linkinghub.elsevier.com/retrieve/pii/0017931070901146.
[34] M.M. Shah, Chart correlation for saturation boiling heat transfer: Equation and further study, ASHREA Trans. 88 (1982) https://www.osti.gov/scitech/biblio/6051573.
[35] J.Y. Shin, M.S. Kim, S.T. Ro, Experimental study on forced convective boiling heat transfer of pure refrigerants and refrigerant mixtures in a horizontal tube, Int. J. Refrig. 20 (1997) 267–275, https://doi.org/10.1016/S0140-7007(97)00004-2.
[36] K. Stephan, Heat transfer in condensation and boiling, Springer, 1992.
[37] L. Sun, K. Mishima, Evaluation analysis of prediction methods for two-phase flow pressure drop in mini-channels, Int. J. Multiph. Flow 35 (2008) 47–54, https://doi.org/10.1016/j.ijmultiphaseflow.2008.08.003, https://catatanstudi.files.wordpress.com/2009/11/2009-evaluation-analysis-of-prediction-methods-for-2-phase-flow-pressure-drop-in-mini-channels_sun.pdf.
[38] W. Tang, W. Li, A new heat transfer model for flow boiling of refrigerants in micro-fin tubes, Int. J. Heat Mass Transf. 126 (2018) 1067–1078, https://doi.org/10.1016/j.ijheatmasstransfer.2018.06.066, https://linkinghub.elsevier.com/retrieve/pii/S0017931018315539.
[39] B. Thonon, A review of hydrocarbon two-phase heat transfer in compact heat exchangers and enhanced geometries, Int. J. Refrig. 31 (2008) 633–642, https://www.sciencedirect.com/science/article/pii/S014070070800039X https://ac.els-cdn.com/S014070070800039X/1-s2.0-S014070070800039X-main.pdf?_tid=7736d389-b443-4b35-8ffb-50ac91ad354f&acdnat=1536823364_5438da16af606309302c7cfda3040a78.
[40] T.N. Tran, M.W. Wambsganss, D.M. France, Small circular- and rectangular-channel boiling with two refrigerants, Int. J. Multiph. Flow 22 (1996) 485–498, https://doi.org/10.1016/0301-9322(96)00002-X.
[41] M.-Y. Wen, K.-J. Jang, C.-Y. Ho, The characteristics of boiling heat transfer and pressure drop of R-600a in a circular tube with porous inserts, Appl. Therm. Eng. 64 (2014) 348–357, https://doi.org/10.1016/j.applthermaleng.2013.12.074, http://ac.els-cdn.com/S135943111300971X/1-s2.0-S135943111300971X-main.pdf?_tid=2640400c-92fe-11e7-a53a-00000aacb360&acdnat=1504700773_37ab47261a748685ff5d60c858095227.
[42] Y. Xu, X. Fang, A new correlation of two-phase frictional pressure drop for evaporating flow in pipes, Int. J. Refrig. 5 (2012) 2039–2050, https://doi.org/10.1016/j.ijrefrig.2012.06.011, https://www.sciencedirect.com/science/article/pii/S0140700712001570.
[43] Z. Yang, M. Gong, G. Chen, X. Zou, J. Shen, Two-phase flow patterns, heat transfer and pressure drop characteristics of R600a during flow boiling inside a horizontal tube, Appl. Therm. Eng. 120 (2017) 654–671, https://doi.org/10.1016/j.applthermaleng.2017.03.124.